Nonlocal-in-time tail effects in gravitational scattering to fifth post-Minkowskian and tenth self-force orders

Christoph Dlapa,[1,*] Gregor Kälin,[2,†] Zhengwen Liu,[3,‡] and Rafael A. Porto[4,§]

[1]*II. Institute for Theoretical Physics, Hamburg University, D-22761 Hamburg, Germany*
[2]*Institute for Theoretical Physics, ETH Zürich, 8093 Zürich, Switzerland*
[3]*School of Physics and Shing-Tung Yau Center, Southeast University, Nanjing 210096, China*
[4]*Deutsches Elektronen-Synchrotron DESY, Platanenallee 6, 15738 Zeuthen, Germany*

(Received 4 May 2026; accepted 3 June 2026; published 10 July 2026)

Using the worldline effective field theory formalism, we derive the nonlocal-in-time conservative contributions arising from tail effects in gravitational scattering to the fifth post-Minkowskian (5PM) and tenth self-force (10SF) orders. The result features multiple polylogarithms of up to weight 3. This challenging computation relies on state-of-the-art integration techniques, including a novel integration-by-parts algorithm: the "Sparse Integral Reducer" (SpIdER). We find perfect agreement in the overlap with all existing literature through the sixth post-Newtonian order. The results presented here provide a key ingredient for isolating the local-in-time component of the conservative two-body dynamics of binary inspirals at the 5PM order.

DOI: 10.1103/wkp4-vy6g

I. INTRODUCTION

The advent of gravitational wave (GW) astronomy, together with ambitious future observatories such as LISA [1], Cosmic Explorer [2], and the Einstein Telescope [3], has restored the relativistic two-body problem in general relativity into a central role [4]. Much of the recent progress is organized around two complementary viewpoints. On the one hand, in the post-Newtonian (PN) regime, we compute observables simultaneously through an expansion in the relative velocity and in G, Newton's constant. On the other hand, in the post-Minkowskian (PM) approximation, we fix instead an order in G but retain full velocity dependence. In the last several years, both approaches have progressed at an exceptional pace (see, e.g., Refs. [5–74]), with the combination of worldline effective field theory (WEFT) methodologies [75–83] and integration toolkits developed in collider physics (e.g., Refs. [57–60,84–86]) playing a major role.

From the weak-field and slow-velocity perspective, the dynamics is known in full through the 4PN order [5–9,11–14], while at 5PN, both the potential sector and nonlinear radiation-reaction and hereditary contributions are under control [15–18,25,26,87], together with partial knowledge also at higher orders [21–23,88,89]. In the PM regime, which is particularly natural for scattering computations, the total spacetime impulse has been obtained through 4PM [51,52], including spin effects [90,91]. At the 5PM order, the calculations have been carried out in concert with a self-force (SF) expansion in a small mass ratio and pushed through 5PM/2SF order [67,68,74]. Yet, the 5PM/2SF scattering results obtained in Ref. [74] are fixed only up to the value of two boundary integrals in the "memory" region, reflecting the subtleties associated with nonlinear conservative effects [87].

For all of this progress, a conceptual obstruction still remains when attempting to convert scattering information into observables for gravitationally bound systems. The full PM results of Refs. [51,52,67,68,74], by themselves, do not yield the correct bound dynamics upon analytic continuation via the "boundary-to-bound" (B2B) dictionary [37–39]. The source of this failure, however, is well understood: nonlocal-in-time tail terms [5,6] that arise from the scattering of the emitted GW radiation off the binary's own long-range (static) field.[1] These hereditary effects obstruct the naive use of unbound data to describe generic elliptic motion.

A resolution of this problem within the PM domain was recently developed in Ref. [63], and extended to the 5PM/1SF level in Ref. [64]. Starting from the complete 4PM [51,52] and 5PM/1SF [67,68] sectors, the universal (local)

*Contact author: christoph.dlapa@desy.de
†Contact author: kaeling@phys.ethz.ch
‡Contact author: zhengwen.liu@seu.edu.cn
§Contact author: rafael.porto@desy.de

Published by the American Physical Society under the terms of the Creative Commons Attribution 4.0 International license. Further distribution of this work must maintain attribution to the author(s) and the published article's title, journal citation, and DOI. Funded by SCOAP³.

[1]Other types of nonlocal-in-time hereditary contributions, such as *tail-of-tail* effects, also contribute to the conservative part of the dynamics [71]. We do not compute these terms here.

part of the conservative dynamics was isolated via an explicit calculation of nonlocal tail contributions to gravitational scattering. The purpose of the present paper is to carry this program substantially further. Instead of truncating at the leading SF order, we derive the $\mathcal{O}(G^5)$ nonlocal-in-time tail corrections to gravitational scattering through the tenth order in the mass-ratio expansion.

Following Refs. [57,63,64], our calculations are organized using the methodology of differential equations combined with a novel integration-by-parts (IBP) algorithm: the "Sparse Integral Reducer" (SpIcaR), designed to handle the large (absolute) powers of linear propagators involved due to the mass-ratio expansion. The nonlocal tail contributions to the deflection angle to 5PM/10SF can then be shown to depend on multiple polylogarithms up to weight 3. We find agreement in the overlap with state-of-the-art derivations in the PN literature through the 6PN order [23]. The results presented here supply one of the key inputs needed to isolate the local-in-time contribution to the conservative dynamics of binary inspirals through the 5PM/10SF order. We briefly comment on the necessary steps and will return to this issue elsewhere.

II. NONLOCAL TAIL EFFECTS

At leading order in the tail expansion, nonlocal contributions to gravitational scattering are governed by an integral over the (source) energy spectrum multiplied by a logarithm of the center-of-mass GW frequency. This has been observed in Refs. [5,6] within the PN domain, and explicitly demonstrated in Ref. [39] in the PM regime [see also Ref. [19] for recent results at $\mathcal{O}(G^7)$]. The nonlocal part of the radial action then takes the factorized form [39]

$$\mathcal{S}_r^{(\mathrm{nloc})} = -\frac{GE}{2\pi}\int_{-\infty}^{+\infty}\frac{d\omega}{2\pi}\frac{dE_{\mathrm{src}}}{d\omega}\log[(2e^{\gamma_E}GM\omega)^2]. \quad (1)$$

We adopt the conventions of Ref. [63]: E denotes the total energy, $\frac{dE_{\mathrm{src}}}{d\omega}$ is the (odd-in-velocity) source GW spectrum in the center-of-mass frame, $M = m_1 + m_2$ is the total mass, and γ_E is Euler's constant. The scattering angle satisfies $\frac{\chi}{2\pi} = -\partial_J \mathcal{S}_r$, with J being the total angular momentum. Writing the conservative deflection angle in the PM approximation, we parametrize its coefficients as

$$\frac{\chi}{2} = \sum_{n=1}^{n=5}\left(\chi_b^{(n)} + \chi_b^{(n)\log}\log\frac{\hat{b}}{\Gamma}\right)\hat{b}^{-n} \quad (2)$$

to leading order in the tail expansion. We introduce $\hat{b} \equiv b/GM$, with b being the impact parameter, $\gamma \equiv u_1 \cdot u_2$, with u_a ($a = 1, 2$) as the incoming four-velocities, and we use a mostly negative metric convention. We also define $\Gamma \equiv E/M = \sqrt{1 + 2\nu(\gamma - 1)}$, with $\nu \equiv m_1 m_2/M^2$.

While the total expression for ratio χ/Γ is known to truncate in the ν expansion [37,40], that is not the case for the nonlocal part. This is due to the integrand in Eq. (1) carrying nontrivial dependence on both the relative velocity and the mass ratio [63]. Therefore, we adopt the same strategy as in Ref. [64], and we expand the integrand in powers of the small mass ratio, $m_2/m_1 \ll 1$, which is directly associated with the traditional SF expansion. As already shown in Ref. [63], the logarithmic contribution admits an SF-exact representation, which was already obtained at the 5PM order in Ref. [64]. We compute here the remaining nonlocal tail contributions to $\chi_b^{(5)}/\Gamma$ through the 10SF order.

III. BUILDING THE INTEGRAND

The integrand for the nonlocal part of the radial action [Eq. (1)] has already been constructed in Ref. [64]. Using a partial fraction decomposition, together with relabeling symmetries, we embed all the relevant scalar integrals into a single integral family. The family is defined by three delta functions in $\{\ell_1 \cdot u_1,\ \ell_2 \cdot u_1,\ \ell_3 \cdot u_2\}$, a set of linear propagators, $\{\ell_1 \cdot u_2, \ell_2 \cdot u_2, \ell_3 \cdot u_1\}$, and it is completed by a choice of square propagators, $\{-\ell_1^2,\ -\ell_2^2,\ -\ell_3^2,\ -(\ell_1 - q)^2,\ -(\ell_2 - q)^2,\ -(\ell_3 - q)^2,\ -(\ell_1 - \ell_2)^2,\ -(\ell_2 - \ell_3)^2,\ -(\ell_3 - \ell_1)^2\}$. A set of sample topologies from this integral family is displayed in Fig. 1. The nontrivial mass dependence enters through the factor of $\log[\omega^2] = \log[(k \cdot u_{\mathrm{com}})^2]$, with

$$u_{\mathrm{com}} \equiv \frac{m_1 u_1 + m_2 u_2}{M\Gamma}, \quad (3)$$

and k^μ denotes a radiation mode, characterized by being the only on-shell mode in a given integral. We identify two such integration regions, which we refer to as the "1 rad" regions [57], with $k_{(1)} = \ell_2 - \ell_3$, $k_{(2)} = \ell_1 - \ell_3$. The restriction to the 1 rad regions follows from the fact that this is the region contributing to the source energy spectrum entering in Eq. (1). As it turns out, the existence of two independent 1 rad regions plays an important role in the computation of the relevant integrals. Upon expansion in the small mass ratio, $m_2/m_1 \ll 1$,

$$\begin{aligned}&\log[(k \cdot u_{\mathrm{com}})^2] \\ &= \log[(k \cdot u_1)^2] - 2\sum_{n=1}^{\infty}\frac{(-1)^n}{n}\left(\frac{k \cdot u_2}{k \cdot u_1}\right)^n\left(\frac{m_2}{m_1}\right)^n \\ &\quad - 2\log\left[\left(1 + \frac{m_2}{m_1}\right)\Gamma\right], \end{aligned} \quad (4)$$

such that the computation can then be split into three separate parts according to the three lines of Eq. (4).

The logarithm in the last line is independent of the loop momenta and therefore simply multiplies the total radiated energy computed in Ref. [52]. On the other hand, the contribution of the logarithm in the first line was obtained in Ref. [64] by treating the latter as a standard linear

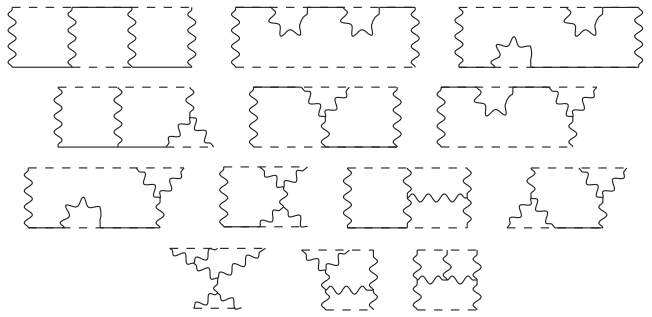


FIG. 1. Sample scalar top-sector integral topologies. Wavy lines represent graviton propagators, solid lines indicate (linear) worldline propagators, and dashed lines denote cut (linear) worldline propagators (delta functions).

propagator with noninteger power—i.e., $(k \cdot u_1)^{2\tilde{\epsilon}}$—and successively keeping only the part linear in $\tilde{\epsilon}$. It is convenient to distinguish $\tilde{\epsilon}$ from the standard $\epsilon \equiv (3-d)/2$ introduced in dimensional regularization. (Due to the method of regions and delta functions, it is also convenient to expand around $d = 3$ rather than $d = 4$.) The main goal of this paper is to compute the contributions from the additional terms in the second line up to an overall 10SF order.

IV. SPARSE INTEGRAL REDUCER

After the full answer is written as a series of Feynman integrals, we exploit linear relations to write them in terms of a set of master integrals. This not only vastly reduces the total number of integrals that needs to be computed, but also facilitates the subsequent computation of the master integrals through the method of differential equations. This so-called IBP reduction is by now a standard procedure in high-energy physics and is implemented in various publicly available computer codes, such as `Kira` [84], `Fire` [85], and `LiteRed` [86].

At leading order in the SF expansion [64], the `Kira` algorithm was able to deal with the powers of $\tilde{\epsilon}$ in the exponents after some minor modifications. Yet, although the scalar integrals belong to the same family as those considered in Refs. [52,57] for the computation of the impulse, the higher-order corrections in the mass ratio involve increasingly large powers of the linear propagators, which reach ± 12 at the 10SF order. In this regime, a naive Laporta-style reduction becomes cumbersome, as the large index ranges translate directly into substantial runtime and memory demands. A different strategy was therefore needed to be able to progress beyond the leading SF order.

In order to address these issues, we introduced the new SPICAR program. The latter is built on a modified version of the strategy implemented in `LiteRed` [86]. Unlike the traditional Laporta approach, SPICAR constructs *symbolic* reduction rules at the level of sectors, rather than solving only for a predetermined list of target integrals. The derivation of these rules is largely independent of the specific subset of integrals that ultimately appears in the calculation: any integral within the covered sectors can be reduced subsequently by straightforward rule application. This feature is particularly valuable at higher orders in the perturbative expansion, where the full set of required integrals is not known *a priori* in closed form and increases significantly with each order.

The advantage of symbolic rules is that they effectively remove the "forward-solving" (and seeding) stage, which often constitutes a major bottleneck in Laporta implementations. Once symbolic reduction rules are available, a minimal forward-solved (upper triangular) form of the IBP system can be constructed by recursively traversing the dependency tree associated with the set of target integrals. In our setup, master integrals are identified precisely as those to which no symbolic rule applies—i.e., the integrals corresponding to columns without a pivot element. The precise form and size of the forward-solved system depend strongly on the chosen integral ordering.[2]

The computational challenge is shifted to the *application* of the symbolic rules and the reduction of large integral expressions. For this purpose, we developed a dedicated engine based on a bottom-up strategy for sparse back substitution, using finite-field arithmetic (FF) and rational reconstruction (RR). More concretely, reductions are performed over suitable prime fields, where algebraic operations are fast and the growth of intermediate expressions is tightly controlled. The resulting data are then combined via RR to recover the exact rational coefficients. This approach allows us to navigate an intermediate reduction graph containing order-10^8 integrals, while explicitly computing the associated reduction coefficients. In practice, FF and RR techniques ensure that the computational cost is dominated by modular numerical back-substitution of a sparse matrix and by RR, rather than by large rational symbolic arithmetic at intermediate stages. This made it possible to perform the computation entirely in main memory, without resorting to disk-based storage. Moreover, the numerical reduction can be straightforwardly parallelized, with negligible overhead and minimal need for synchronization.

Finally, at tenth order in the expansion, we also encounter additional sectors beyond those appearing at leading order in Ref. [64]. Although conceptually straightforward, this introduces a number of new masters. This enlargement turns out to be important, as it requires extending the rule-generation step to cover the relevant topologies. Once these are incorporated, the full set can be treated uniformly within the same framework. The SPICAR algorithm successfully generated symbolic rules for all sectors needed in our calculation.

[2]By incorporating ideas to improve the symbolic reduction rules similar to those in Ref. [92]—which can be implemented straightforwardly within the SPICAR algorithm—we can in principle reduce the size of the forward-solved system even further.

V. INTEGRATION

For the computation of the master integrals, we follow the approach outlined in detail in Ref. [57]: We derive differential equations in x, given by $\gamma = \frac{1}{2}(x + \frac{1}{x})$ and transform them to canonical form [93]. The differential equations possess the same structure as the ones we encountered before in Refs. [52,57], with the exception of a few extra master integrals. We note that, for the leading term in the SF expansion, it is advantageous to temporarily set $\tilde{\epsilon} = \eta\epsilon$ before deriving canonical differential equations that are factorized in ϵ. For this task, we use private codes which deal with the η parameter.

The solution of the differential equations depend on multiple polylogarithms (MPLs) up to transcendental weights 3 and 2, for the leading and higher-order SF terms, respectively. The MPLs are defined through the relation

$$G(a_1,\ldots,a_n;z) = \int_0^z \frac{dt}{t-a_1} G(a_2,\ldots,a_n;t),$$
$$G(\cdot;z) = 1, \qquad G(\underbrace{0,\ldots,0}_{n};z) = \frac{1}{n!}\log^n z, \tag{5}$$

with (a_n, z) being complex numbers. The increased weight of the leading term may be attributed to the fact that the logarithm in the first line of Eq. (4) has weight 1, thus increasing the maximum weight relative to the other terms. Furthermore, elliptic integrals are completely absent, since they appear only in the direction of the impact parameter at $\mathcal{O}(G^4)$. The result can be written in terms of a five letter *alphabet*, $a_i \in \{0, 1, 2, 1 \pm i\}$. We choose the variable $z = 1 - x$, which has a direct connection with the PN expansion, and furthermore it allows us to efficiently determine an independent set of boundary constants using the methods developed in Ref. [57].

The integration problem then reduces to the computation of boundary conditions in the $z \to 0$ ($\gamma \to 1$) limit, characterized in our case by a single propagator going on shell. An expansion in small velocity leads to a factorization of the full three-loop integrals into an (outer) two-loop integral times an (inner) tadpole, which only talk to each other through the dependence on the argument of a single linear propagator $\boldsymbol{\ell}_i \cdot \boldsymbol{n}$. The $\boldsymbol{\ell}_i$ is one of the two outer integration momenta, and $\boldsymbol{n}$ is chosen such that $\boldsymbol{\ell} \cdot \boldsymbol{n} = \ell_z$.

The tadpole integral is known analytically for any power of the single propagator, and it evaluates to a result proportional to $(\boldsymbol{\ell}_i \cdot \boldsymbol{n})^d$. The dependence on d, as well as the introduction of the $\tilde{\epsilon}$ parameter to handle the leading logarithmic-dependent term, implies noninteger powers for one of the linear propagators of the outer integrals, which can all be embedded into the following family:

$$\boldsymbol{I}^{\pm\pm}_{a_1a_2;a_3a_4a_5a_6a_7} = \int \frac{e^{2\gamma_{\rm E}\epsilon}}{\pi^d} \frac{\mathrm{d}^d\boldsymbol{\ell}_1 \mathrm{d}^d\boldsymbol{\ell}_2}{(\boldsymbol{\ell}_1\cdot\boldsymbol{n} \pm i0)^{a_1}(\boldsymbol{\ell}_2\cdot\boldsymbol{n} \pm i0)^{a_2}(\boldsymbol{\ell}_1^2)^{a_3}(\boldsymbol{\ell}_2^2)^{a_4}} \times \frac{1}{((\boldsymbol{\ell}_1-\boldsymbol{q})^2)^{a_5}((\boldsymbol{\ell}_2-\boldsymbol{q})^2)^{a_6}((\boldsymbol{\ell}_1-\boldsymbol{\ell}_2)^2)^{a_7}}, \tag{6}$$

with $\boldsymbol{q}\cdot\boldsymbol{n} = 0$, $a_{i\neq 1}$ integer numbers, and $a_1 = \mathbb{Z} + \mathcal{O}(\epsilon, \tilde{\epsilon})$.

These integrals fulfill similar IBP identities to their $(d+1)$-dimensional counterparts. The algorithm implemented in SPIDER is able to produce a complete set of symbolic rules that allows a reduction of all relevant integrals in this family into the following master integrals:

$$\boldsymbol{I}^{-+}_{(1+2\epsilon-2\tilde{\epsilon})1;10011}, \quad \boldsymbol{I}^{+\pm}_{(2\epsilon-2\tilde{\epsilon})0;10011}, \quad \boldsymbol{I}^{++}_{(1+2\epsilon-2\tilde{\epsilon})1;10011},$$
$$\boldsymbol{I}^{-+}_{(2\epsilon)1;10011}, \quad \boldsymbol{I}^{-+}_{(1+2\epsilon)1;10011}, \quad \boldsymbol{I}^{-+}_{(1+2\epsilon)1;10101},$$
$$\boldsymbol{I}^{+\pm}_{(2\epsilon)0;10011}, \quad \boldsymbol{I}^{++}_{(2\epsilon)1;10011}, \quad \boldsymbol{I}^{+\pm}_{(-1+2\epsilon)0;10011},$$
$$\boldsymbol{I}^{++}_{(1+2\epsilon)1;10011}, \quad \boldsymbol{I}^{++}_{(1+2\epsilon)1;10101}, \tag{7}$$

which are sufficient to all SF orders. We find complete analytic results through a Schwinger parametrization and iterated integration of the Schwinger parameters. Some examples of similar boundary integrals—including a thorough discussion of many of the finer details—can be found in Refs. [57,94]. For the readers' convenience, we list their values and ϵ-expanded forms in Appendix A.

VI. SCATTERING DATA

Combining the leading (nonlogarithmic) SF contribution from Red. [64] with the newly obtained results in this paper, we find the following structure:

$$\frac{\chi^{(5)(10\ \mathrm{SF})}_{b(\mathrm{nloc})}}{\Gamma\nu} = \sum_{i=1}^{26} [h_i^{(0)}(x) + h_i^{(1)}(x)\nu^1 + \sqrt{1-4\nu}\, h_i^{(1/2)}(x) + \Delta h_i(x,\nu)]\mathcal{G}_i(x), \tag{8}$$

for the coefficient of the scattering angle in Eq. (2), where $h_i^{(0,1,1/2)}$ are rational functions of x only, and $\Delta h_i(x,\nu)$ are rational in x and polynomial in ν, starting at $\mathcal{O}(\nu^2)$ and ranging up to $\mathcal{O}(\nu^9)$. Furthermore, the $\Delta h_i(x,\nu)$ vanish except for $i = 1, 3, 4, 6, 7, 8$. See Ref. [95] for (computer-readable) explicit expressions. The combinations of MPLs in the $\mathcal{G}_i(x)$'s are listed in Appendix B.

The result in Eq. (8), together with the SF-exact logarithmic pieces [64], completes the knowledge of nonlocal tail-like contributions to 5PM/10SF order. For the sake of comparison, expressing the scattering angle including the logarithmic terms as a function of the reduced angular momentum, $\chi = \sum_n 2\chi_j^{(n)} j^{-n}$, with $j = J/(GM^2\nu)$, $v_\infty = \sqrt{\gamma^2-1}$, and expanding to the 10PN order, we find

$$\chi^{(5)(10\,\mathrm{PN})}_{j(\mathrm{nloc})} = \frac{\nu v_\infty^3}{2}\left\{-\frac{5440}{27}-\frac{25088}{45}\log\left(\frac{2v_\infty}{\sqrt{j}}\right)+v_\infty^2\left[\left(\frac{55808\nu}{45}-\frac{297728}{525}\right)\log\left(\frac{2v_\infty}{\sqrt{j}}\right)+\frac{155200\nu}{189}+\frac{374368}{2625}\right]\right.$$
$$+v_\infty^4\left[\left(-\frac{86528\nu^2}{45}+\frac{1152896\nu}{1575}-\frac{3525568}{11025}\right)\log\left(\frac{2v_\infty}{\sqrt{j}}\right)-\frac{7750528\nu^2}{4725}-\frac{41361872\nu}{165375}+\frac{166150088}{385875}\right]$$
$$+v_\infty^6\left[\left(\frac{117248\nu^3}{45}-\frac{875008\nu^2}{1575}+\frac{3096256\nu}{6615}+\frac{2429664}{13475}\right)\log\left(\frac{2v_\infty}{\sqrt{j}}\right)\right.$$
$$\left.+\frac{1046272\nu^3}{405}+\frac{21978496\nu^2}{33075}-\frac{22499132024\nu}{38201625}+\frac{1137056876}{7640325}\right]$$
$$+v_\infty^8\left[\left(-\frac{147968\nu^4}{45}+\frac{3968\nu^3}{105}-\frac{886048\nu^2}{1323}-\frac{279650936\nu}{363825}+\frac{1620350092}{2477475}\right)\log\left(\frac{2v_\infty}{\sqrt{j}}\right)\right.$$
$$\left.-\frac{80567008\nu^4}{22275}-\frac{2743988288\nu^3}{1819125}+\frac{204678995432\nu^2}{420217875}-\frac{3137954156509\nu}{5462832375}+\frac{38172272288071}{120182312250}\right]$$
$$+v_\infty^{10}\left[\left(\frac{178688\nu^5}{45}+\frac{1293568\nu^4}{1575}+\frac{1289632\nu^3}{1225}+\frac{16506176\nu^2}{11025}-\frac{307880492\nu}{315315}-\frac{735017339222}{676350675}\right)\log\left(\frac{2v_\infty}{\sqrt{j}}\right)\right.$$
$$+\frac{1367324512\nu^5}{289575}+\frac{18434632624\nu^4}{6449625}+\frac{75486806288\nu^3}{2630252625}+\frac{88618604658512\nu^2}{71016820875}-\frac{308380410342341\nu}{426100925250}$$
$$\left.-\frac{81515761234704829}{121864864621500}\right]$$
$$+v_\infty^{12}\left[\left(-\frac{209408\nu^6}{45}-\frac{3184256\nu^5}{1575}-\frac{57721472\nu^4}{33075}-\frac{98860192\nu^3}{40425}+\frac{48577741364\nu^2}{52026975}+\frac{525179938397\nu}{225450225}\right.\right.$$
$$\left.+\frac{108812096826773}{68987768850}\right)\log\left(\frac{2v_\infty}{\sqrt{j}}\right)-\frac{1704352288\nu^6}{289575}-\frac{338314320616\nu^5}{70945875}-\frac{245498965780408\nu^4}{213050462625}$$
$$\left.\left.-\frac{486269791848056\nu^3}{213050462625}+\frac{2009480696060767\nu^2}{2343555088875}+\frac{25168487123370619421\nu}{12430216191393000}+\frac{27550186358971497707}{24860432382786000}\right]\right\}. \tag{9}$$

As stressed in Ref. [63], the nonlocal-in-time contribution defined in Refs. [22,23] contains, besides Eq. (1)—denoted W_1 in Ref. [23]—an additional term (W_2) given by a time integral involving $\frac{dE}{dt}$ weighted by $\log r(t)$. This (coordinate-dependent) term arises from quasi-instantaneous, potential-region interactions, and therefore we do not assign it to the nonlocal-in-time sector. Upon comparing the expression in Eq. (9) with the deflection angle obtained from the W_1-only result of Ref. [23], we find perfect agreement in the overlapping regime of validity to 6PN. The PN-expanded value for the nonlocal-in-time (W_1-only) contribution to the scattering angle at $\mathcal{O}(G^5)$ through the 30PN/10SF order is provided in Ref. [95].

VII. TOWARD THE 5PM GRAVITATIONAL DYNAMICS

The identification of nonlocal-in-time effects in the scattering angle allows us to in principle isolate the universal part of the conservative dynamics entirely within the PM framework. This strategy was followed in our previous work at the 4PM [63] and 5PM/1SF [64] orders. Using the B2B dictionary [37–39], the resulting Hamiltonian applicable for elliptic motion through the 5PM order can be separated into local- and nonlocal-in-time contributions as follows [64]:

$$\hat{H}^{\mathrm{ell}}_{\mathrm{5PM}} = \hat{E}_0 + \sum_{i=1}^{i=5}\frac{\hat{c}_{i(\mathrm{loc})}}{\hat{r}^i} + \sum_{i=1}^{i=5}\frac{\hat{c}_{i(\mathrm{nloc})}}{\hat{r}^i} - G\sum_{i=4}^{i=5}\left(\hat{H}\frac{dE_{\mathrm{src}}}{dt}\right)\Big|_{(i-1)\mathrm{PM}}\log\left(\frac{\hat{r}}{e^{2\gamma_E}}\right), \tag{10}$$

with $\hat{H}\equiv\frac{H}{M\nu}$, $\hat{r}=\frac{r}{GM}$, and $\hat{E}_0\equiv\frac{1}{M\nu}\sum_a\sqrt{\boldsymbol{p}^2+m_a^2}$ as the normalized kinetic term. The $\hat{c}_{1|2|3(\mathrm{loc})}$ are the PM-exact coefficients through $\mathcal{O}(G^3)$ computed in Refs. [34,36,41,42], with $\gamma=(E_1E_2+\boldsymbol{p}^2)/m_1m_2$. The coefficient $\hat{c}_{4(\mathrm{loc})}$ was obtained in Ref. [63] to all SF orders, while the 5PM coefficient $\hat{c}_{5(\mathrm{loc})}$ was derived in Ref. [64] at the 1SF level. The factor multiplying $\log(\frac{\hat{r}}{e^{2\gamma_E}})$ in Eq. (10) can be shown to depend on lower-order $\hat{c}_i$'s combined with the source

("1 rad"-only) energy flux. The relation follows from the general structure in Eq. (1), including the factor of GE, together with the cancellation in the dimensional regularization of ultraviolet and infrared divergences—and associated $\log b$ terms—between local- and nonlocal-in-time contributions [6,39,50,63]. For the bound Hamiltonian to the 5PM order, this implies the structure

$$\left(\hat{H}\frac{dE_{\rm src}}{dt}\right)\Big|_{G^4} = \left(\frac{\hat{c}_1}{\hat{r}}\frac{dE_{\rm src}}{dt}\Big|_{G^3} + \hat{E}_0\frac{dE_{\rm src}}{dt}\Big|_{G^4}\right), \qquad (11)$$

which is displayed in front of the logarithm in the second line of Eq. (10). The explict values for the source energy fluxes are given in Refs. [50,63] at $\mathcal{O}(G^3)$, and the 4PM component can be found in Ref. [64].

The remaining nonlogarithmic contributions, $\hat{c}_{i(\rm nloc)}$, are not known in a PM framework for elliptic motion. Closely related coefficients, albeit in a different gauge, have been computed in the PN approximation via a small-eccentricity expansion through the 6PN order [22,23]. These results can be easily translated to an isotropic gauge by extending the analysis performed in Ref. [64].

Armed with the nonlocal-in-time correction to the scattering angle at the 5PM/10SF order computed in this paper, and following the same sequence of manipulations as in Refs. [63,64], it would in principle be straightforward to extract the corresponding contribution to $\hat{c}_{5(\rm loc)}$ through the same 5PM/10SF order, provided the value of the *full* conservative scattering angle at $\mathcal{O}(G^5)$ is at hand. Significant progress in this direction was reported in Ref. [74]. However, while the potential and tail-like regions are under control, several subtleties associated with memory-like contributions prevent the conservative value of the total scattering angle from being fully settled [87]. Nevertheless, it is still useful to split the 5PM coefficient into two pieces:

$$\hat{c}_{5(\rm loc)} = \hat{c}^{(\rm P+T)}_{5(\rm loc)} + \hat{c}^{(\rm M)}_{5(\rm loc)}, \qquad (12)$$

where the potential-plus-tail part, $\hat{c}^{(\rm P+T)}_{5(\rm loc)}$, starts at $\mathcal{O}(\nu)$, and the memory-like piece, $\hat{c}^{(\rm M)}_{5(\rm loc)}$, enters at $\mathcal{O}(\nu^2)$. Using the results in Ref. [74], we can then extend our analysis in Ref. [64] and determine $\hat{c}^{(\rm P+T)}_{5(\rm loc)}$ through the 10SF order. The remaining memory-like contribution can be incorporated through a PN-expanded representation [87], in parallel with the nonlocal tail sector.

Although the Hamiltonian in Eq. (10) is engineered for the bound problem, there is in principle a caveat to this program. Namely, the local-in-time universal component must be analytically continued from the regime of hyperbolic encounters, where the potential-region contribution to the scattering calculation at $\mathcal{O}(G^5\nu^2)$ contains spurious poles at $\gamma = 3$ [74]. If taken at face value, these singularities would feed directly into $\hat{c}^{(\rm P+T)}_{5(\rm loc)}$ starting at the 2SF order, and they cannot be removed by supplementing it with a PN-truncated expression for $\hat{c}^{(\rm M)}_{5(\rm loc)}$.

The authors of Ref. [74] therefore advocated for an alternative definition of the conservative dynamics, the so-called "$\gamma - 3$" prescription, in which a memory-like contribution is constructed as to cancel the singular behavior arising from the potential region. However, as discussed in Ref. [87], this prescription introduces an unnatural sign flip between tail and memory contributions associated with the same term in the effective action, and moreover, if implemented at higher PM orders, it leads to spurious π^2 terms at $\mathcal{O}(G^6\nu^2)$. Alternatively, inspired by Feynman's $i0^+$ prescription, a different routing was advocated in [87] for the memory-like region at the 5PM order. Yet, although devoid of ϵ poles, Feynman's prescription does not appear to remove the singular behavior at $\gamma = 3$.

We envision two possible routes for resolving these issues. First, as advocated in Ref. [87], one natural option is to extend the isotropic-like representation to the full 5PM dynamics. This would require going beyond the impulse alone and deriving, within the same framework, the associated energy and angular-momentum losses, as well as the time delay. Such a construction would be independent of any prior split into conservative and dissipative sectors, and should therefore be free of spurious singularities. In this setting, the nonlocal-in-time tail effects constructed here could also be systematically removed and reinserted at the level of the full dynamics within a PN-expanded framework.

A second possibility is to retain the split into conservative and dissipative contributions, while defining the conservative sector strictly within the domain relevant for bound motion. Since the latter is restricted to $\gamma < 1$, the singular behavior at $\gamma = 3$ is never attained. From this perspective, an all-orders-in-velocity expression for $\hat{c}^{(\rm P+T)}_{5(\rm loc)}$ may still provide an improved description of the two-body bound dynamics—after all, potential interactions find their natural habitat in such a regime.[3] However, it should not be interpreted as an object that can be naively extrapolated to the relativistic limit of unbound motion. We will return to these considerations elsewhere.

VIII. CONCLUSIONS

The combination of modern multiloop integration technology with the WEFT formalism has opened a new

[3]Let us emphasize that, pending a more satisfactory resolution of the issue of infrared divergences associated with Feynman's prescription for scattering events, the 5PM results of Ref. [74] explicitly show that the $1/\epsilon$ poles generated in the potential and tail regions cancel each other out, as expected [10,39]. Furthermore, as argued in Ref. [87], a local-in-time version of Feynman's boundary conditions in the memory region can also be shown to be consistent with the cancellation of poles in dimensional regularization.

analytic window onto gravitational scattering in general relativity, making it possible to compute (gauge-invariant) observables with increasing precision [51,52,67,68,74]. Yet the passage from hyperbolic encounters to bound inspirals is not automatic. As demonstrated in Refs. [37–39], the instantaneous pieces and logarithmic sector possess the expected universal character, whereas the complete scattering answer contains genuinely orbit-dependent nonlocal-in-time information. Without disentangling this hereditary component, the hyperbolic result cannot be directly used to model binaries in nearly circular or mildly eccentric configurations.

The first systematic implementation of such a disentangling within the PM expansion was achieved in Ref. [63] at $\mathcal{O}(G^4)$, where the local dynamics was separated from tail-induced nonlocal effects to all orders in the SF expansion. Building on that construction, in Ref. [64] we extended the decomposition of hereditary terms in the conservative scattering angle at the 5PM/1SF order. Subtracting this piece from the total value in Ref. [67] yields a genuinely instantaneous part of the 5PM dynamics at the 1SF order, which can then be mapped through the B2B dictionary to generic bound motion [37,38].

The purpose of the present paper was to carry this program further by deriving the $\mathcal{O}(G^5)$ nonlocal-in-time tail corrections to gravitational scattering through the 10SF order. This provides a significantly more detailed characterization of the hereditary sector at the 5PM order and supplies the information needed to in principle disentangle, order by order in ν, the local-in-time dynamics from the genuinely nonlocal contribution to the scattering angle. Explicit formulas for the relevant building blocks, together with PN expansions through the 30th order, are provided in Ref. [95].

The results in this paper also pave the path forward to construct the 5PM two-body Hamiltonian for bound motion through the 10SF order. The main remaining issue lies in the treatment of memory-like effects, and in particular how the $\gamma = 3$ singularity induced by potential interactions is ultimately handled. A natural resolution, as advocated in Ref. [87], may require either formulating the full dynamics without splitting into conservative and dissipative pieces, or else interpreting the (resummed) conservative sector strictly within the PN domain of elliptic orbits, where singularities at $\gamma > 1$ remain outside the physical regime of bound motion. We will address these issues in more detail in future work.

Apart from their immediate application to waveform modeling—that is, particular relevance for third-generation GW detectors [1–3]—the plethora of recent results pushing the boundaries of our understanding of gravitational interactions underscores the maturity of the WEFT framework, in both the PN [81–83] and PM domains [41–48], as a systematic approach to the two-body problem in general relativity. In combination with powerful integration tools—e.g., Refs. [57–60,84–86]—it offers a systematic route to navigate through the increasingly intricate integration problem that governs the relativistic binary dynamics. In this direction, the newly developed SPICAR program provides a powerful computational engine for future calculations, and we expect it to play a central role in unlocking further breakthroughs at higher PM orders.

ACKNOWLEDGMENTS

G. K. and R. A. P. would like to thank the participants of the Nordita program "Amplitudes, Strong-Field Gravity and Resummation" for discussions. The work of C. D. is funded by the Deutsche Forschungsgemeinschaft (DFG, German Research Foundation)—Project No. 555751285. R. A. P. acknowledges support by the DFG under Germany's Excellence Strategy—EXC 2121 "Quantum Universe"—No. 390833306. The work of Z. L. was supported partially by the European Union's Horizon Europe research and innovation program under Marie Skłodowska-Curie Grant Agreement No. 101146918 "GWtheory" and by the Start-up Research Fund of Southeast University No. RF1028624160.

DATA AVAILABILITY

The data that support the findings of this article are openly available in the ancillary files [95].

APPENDIX A: BOUNDARY INTEGRALS

We list here the results for the required boundary integrals. The answers contain generalized hypergeometric functions of type ${}_4F_3(z)$ with ϵ-dependent arguments evaluated at $z = 1$:

$$
\begin{aligned}
\boldsymbol{I}^{-+}_{(2\epsilon)1;10011} = {} & \frac{i\pi^2 4^{4\epsilon+1} e^{2\gamma_{\mathrm{E}}\epsilon+i\pi\epsilon} \sin(\pi\epsilon)(\csc(2\pi\epsilon)+\csc(4\pi\epsilon))\Gamma(\frac{1}{2}-3\epsilon)\Gamma(6\epsilon)}{\Gamma(\frac{3}{2}-2\epsilon)\Gamma(-\epsilon)\Gamma(4\epsilon+1)} {}_4F_3\left(\begin{matrix}1-4\epsilon,\frac{1}{2}-3\epsilon,\frac{1}{2}-2\epsilon,\frac{1}{2}-\epsilon\\ 1-6\epsilon,1-2\epsilon,\frac{3}{2}-2\epsilon\end{matrix}\middle|1\right) \\
& - \frac{\pi^{7/2}(4^{6\epsilon}-1)e^{2\gamma_{\mathrm{E}}\epsilon}\epsilon(\tan(\pi\epsilon)-i)\csc(4\pi\epsilon)(\sec(\pi\epsilon)+\sec(3\pi\epsilon))}{\Gamma(1-4\epsilon)\Gamma(\frac{1}{2}-2\epsilon)\Gamma(2\epsilon+1)^2\sinh(\epsilon\log(64))} {}_4F_3\left(\begin{matrix}\frac{1}{2},1-2\epsilon,\frac{1}{2}-\epsilon,\epsilon+\frac{1}{2}\\ \frac{3}{2},1-4\epsilon,2\epsilon+1\end{matrix}\middle|1\right) \\
& - \frac{i\pi 64^{\epsilon} e^{2\gamma_{\mathrm{E}}\epsilon+i\pi\epsilon}\cos(4\pi\epsilon)\Gamma(\frac{1}{2}-2\epsilon)\Gamma(4\epsilon+\frac{1}{2})}{\epsilon-2\epsilon\cos(2\pi\epsilon)},
\end{aligned}
$$

$$
\begin{aligned}
\boldsymbol{I}^{-+}_{(1+2\epsilon)1;10011} &= \frac{i\pi^{3/2}16^{\epsilon}e^{2(\gamma_{\mathrm{E}}+i\pi)\epsilon}\Gamma(-3\epsilon)\Gamma(2\epsilon+\frac{1}{2})\Gamma(6\epsilon+1)(2\cos(2\pi\epsilon)-1)(1+i\cot(\pi\epsilon))}{\Gamma(1-\epsilon)\Gamma(2\epsilon+1)^2}\,{}_4F_3\left(\begin{matrix}\frac{1}{2}-\epsilon,-4\epsilon,-3\epsilon,-2\epsilon\\ \frac{1}{2}-2\epsilon,1-2\epsilon,-6\epsilon\end{matrix}\middle|1\right)\\
&+\frac{4^{3\epsilon+1}e^{2\gamma_{\mathrm{E}}\epsilon+i\pi\epsilon}\sin(8\pi\epsilon)\cos(\pi\epsilon)\Gamma(-2\epsilon-\frac{1}{2})\Gamma(\frac{1}{2}-\epsilon)\Gamma(\epsilon+1)\Gamma(4\epsilon+\frac{1}{2})}{\sqrt{\pi}(2\cos(2\pi\epsilon)+1)\sin(4\pi\epsilon)}\,{}_4F_3\left(\begin{matrix}\frac{1}{2},\frac{1}{2}-2\epsilon,\frac{1}{2}-\epsilon,\epsilon+1\\ \frac{3}{2},\frac{1}{2}-4\epsilon,2\epsilon+\frac{3}{2}\end{matrix}\middle|1\right)\\
&+\frac{\pi^{3/2}2^{4\epsilon+1}e^{2\gamma_{\mathrm{E}}\epsilon+i\pi\epsilon}\Gamma(-\epsilon)(2\cos(\pi\epsilon)\Gamma(-2\epsilon)\Gamma(4\epsilon+1)+\sqrt{\pi}16^{\epsilon}\csc(3\pi\epsilon)\Gamma(2\epsilon+\frac{1}{2}))}{\Gamma(\frac{1}{2}-2\epsilon)\Gamma(\epsilon+1)},\\
\boldsymbol{I}^{-+}_{(1+2\epsilon)1;10101} &= 0,\\
\boldsymbol{I}^{+\pm}_{(2\epsilon)0;10011} &= \frac{\pi^2 4^{\epsilon}e^{2\gamma_{\mathrm{E}}\epsilon-i\pi\epsilon}\csc(3\pi\epsilon)\Gamma(\frac{1}{2}-2\epsilon)\Gamma(\frac{1}{2}-\epsilon)}{\Gamma(\frac{3}{2}-5\epsilon)\Gamma(1-\epsilon)\Gamma(\epsilon+\frac{1}{2})},\\
\boldsymbol{I}^{++}_{(2\epsilon)1;10011} &= -\frac{i\pi^2 2^{8\epsilon+1}e^{2\gamma_{\mathrm{E}}\epsilon-i\pi\epsilon}(2\cos(2\pi\epsilon)+1)\Gamma(\frac{1}{2}-3\epsilon)\Gamma(6\epsilon)}{(\cos(\pi\epsilon)+\cos(3\pi\epsilon))\Gamma(\frac{3}{2}-2\epsilon)\Gamma(-\epsilon)\Gamma(4\epsilon+1)}\,{}_4F_3\left(\begin{matrix}1-4\epsilon,\frac{1}{2}-3\epsilon,\frac{1}{2}-2\epsilon,\frac{1}{2}-\epsilon\\ 1-6\epsilon,1-2\epsilon,\frac{3}{2}-2\epsilon\end{matrix}\middle|1\right)\\
&+\frac{i\pi^{7/2}2^{6\epsilon+1}e^{2\gamma_{\mathrm{E}}\epsilon-3i\pi\epsilon}(1+e^{4i\pi\epsilon})}{(\sin(2\pi\epsilon)+\sin(6\pi\epsilon)+\sin(8\pi\epsilon))\Gamma(\frac{1}{2}-2\epsilon)\Gamma(-4\epsilon)\Gamma(2\epsilon+1)^2}\,{}_4F_3\left(\begin{matrix}\frac{1}{2},1-2\epsilon,\frac{1}{2}-\epsilon,\epsilon+\frac{1}{2}\\ \frac{3}{2},1-4\epsilon,2\epsilon+1\end{matrix}\middle|1\right)\\
&-\frac{i\pi 64^{\epsilon}e^{2\gamma_{\mathrm{E}}\epsilon-i\pi\epsilon}\cos(4\pi\epsilon)\Gamma(\frac{1}{2}-2\epsilon)\Gamma(4\epsilon+\frac{1}{2})}{\epsilon-2\epsilon\cos(2\pi\epsilon)},\\
\boldsymbol{I}^{+\pm}_{(-1+2\epsilon)0;10011} &= -\frac{i\pi 4^{\epsilon}e^{2\gamma_{\mathrm{E}}\epsilon-i\pi\epsilon}\sin(\pi\epsilon)\,\sec(3\pi\epsilon)\Gamma(1-2\epsilon)\Gamma(\frac{1}{2}-\epsilon)}{\Gamma(\frac{5}{2}-5\epsilon)},\\
\boldsymbol{I}^{++}_{(1+2\epsilon)1;10011} &= -\frac{32^{-4\epsilon}e^{2\gamma_{\mathrm{E}}\epsilon-i\pi\epsilon}\sin(2\pi\epsilon)\Gamma(\frac{1}{2}-2\epsilon)\Gamma(-3\epsilon)\Gamma(\epsilon)\Gamma(6\epsilon)}{\sqrt{\pi}}\,{}_4F_3\left(\begin{matrix}\frac{1}{2}-2\epsilon,-4\epsilon,-2\epsilon,2\epsilon+1\\ \frac{1}{2}-3\epsilon,1-2\epsilon,1-\epsilon\end{matrix}\middle|1\right)\\
&+\frac{\pi 4^{4\epsilon+1}e^{2\gamma_{\mathrm{E}}\epsilon-i\pi\epsilon}\sin(2\pi\epsilon)\csc(3\pi\epsilon)\Gamma(-2\epsilon)\Gamma(2\epsilon+\frac{1}{2})}{\epsilon\Gamma(\frac{1}{2}-2\epsilon)}\,{}_4F_3\left(\begin{matrix}\frac{1}{2}-\epsilon,-3\epsilon,-\epsilon,3\epsilon+1\\ \frac{1}{2}-2\epsilon,1-\epsilon,\epsilon+1\end{matrix}\middle|1\right)\\
&-\frac{\pi^{3/2}8^{2\epsilon+1}e^{2\gamma_{\mathrm{E}}\epsilon-i\pi\epsilon}\Gamma(\epsilon+1)\Gamma(5\epsilon+\frac{3}{2})(\sin(4\pi\epsilon)\csc(6\pi\epsilon)-1)}{(4\epsilon+1)\Gamma(\epsilon+\frac{3}{2})\Gamma(3\epsilon+\frac{3}{2})}\,{}_4F_3\left(\begin{matrix}\frac{1}{2}-\epsilon,\epsilon+\frac{1}{2},\epsilon+1,5\epsilon+\frac{3}{2}\\ \epsilon+\frac{3}{2},2\epsilon+\frac{3}{2},3\epsilon+\frac{3}{2}\end{matrix}\middle|1\right),\\
\boldsymbol{I}^{++}_{(1+2\epsilon)1;10101} &= \frac{i\pi^2 4^{2\epsilon+1}e^{2(\gamma_{\mathrm{E}}+i\pi)\epsilon}\Gamma(\frac{1}{2}-\epsilon)}{(-1+e^{6i\pi\epsilon})\epsilon\Gamma(\frac{1}{2}-3\epsilon)},\\
\boldsymbol{I}^{-+}_{(1+2\epsilon-2\tilde{\epsilon})1;10011} &= \frac{\pi^{3/2}4^{1-\epsilon}e^{2\gamma\epsilon+i\pi(\epsilon-\tilde{\epsilon})}\Gamma(\frac{1}{2}-\epsilon)\cos(\pi(3\epsilon-\tilde{\epsilon}))\Gamma(\tilde{\epsilon}-3\epsilon)\Gamma(6\epsilon-2\tilde{\epsilon}+1)}{\sin(2\pi\tilde{\epsilon}-4\pi\epsilon)\Gamma(2\tilde{\epsilon}-4\epsilon+1)\Gamma(-2\tilde{\epsilon}+2\epsilon+1)\Gamma(-\tilde{\epsilon}+2\epsilon+1)}\,{}_4F_3\left(\begin{matrix}2\tilde{\epsilon}-4\epsilon,\tilde{\epsilon}-3\epsilon,\tilde{\epsilon}-2\epsilon,\frac{1}{2}-\epsilon\\ 2\tilde{\epsilon}-6\epsilon,\tilde{\epsilon}-2\epsilon+\frac{1}{2},\tilde{\epsilon}-2\epsilon+1\end{matrix}\middle|1\right)\\
&-\frac{\pi^2 2^{4\epsilon-2\tilde{\epsilon}+2}e^{2\gamma\epsilon+i\pi(\epsilon-\tilde{\epsilon})}\cos(\pi(4\epsilon-\tilde{\epsilon}))\Gamma(\tilde{\epsilon}-2\epsilon-\frac{1}{2})\Gamma(4\epsilon-\tilde{\epsilon}+\frac{1}{2})}{\sin(\pi(3\epsilon-\tilde{\epsilon}))\cos(\pi\epsilon)\Gamma(\epsilon+\frac{1}{2})\Gamma(\tilde{\epsilon}-2\epsilon)\Gamma(-\tilde{\epsilon}+\epsilon+\frac{1}{2})}\,{}_4F_3\left(\begin{matrix}\frac{1}{2},\tilde{\epsilon}-2\epsilon+\frac{1}{2},\frac{1}{2}-\epsilon,\epsilon-\tilde{\epsilon}+1\\ \frac{3}{2},\tilde{\epsilon}-4\epsilon+\frac{1}{2},-\tilde{\epsilon}+2\epsilon+\frac{3}{2}\end{matrix}\middle|1\right)\\
&+\frac{\pi^{7/2}2^{-2\tilde{\epsilon}+4\epsilon+1}e^{2\gamma\epsilon+i\pi(\epsilon-\tilde{\epsilon})}\csc(\pi\epsilon)\sin(\pi(4\epsilon-\tilde{\epsilon}))\csc(\pi(2\epsilon-\tilde{\epsilon}))\csc(\pi(3\epsilon-\tilde{\epsilon}))\Gamma(-\tilde{\epsilon}+4\epsilon+1)}{\Gamma(\epsilon+1)\Gamma(\tilde{\epsilon}-2\epsilon+\frac{1}{2})\Gamma(-\tilde{\epsilon}+\epsilon+1)\Gamma(-\tilde{\epsilon}+2\epsilon+1)},\\
\boldsymbol{I}^{+\pm}_{(2\epsilon-2\tilde{\epsilon})0;10011} &= \frac{\pi^2 4^{\epsilon}e^{2\gamma\epsilon-i\pi(\epsilon-\tilde{\epsilon})}\Gamma(\frac{1}{2}-\epsilon)\csc(3\pi\epsilon-\pi\tilde{\epsilon})\Gamma(-2\epsilon+\tilde{\epsilon}+\frac{1}{2})}{\Gamma(1-\epsilon)\Gamma(\epsilon-\tilde{\epsilon}+\frac{1}{2})\Gamma(-5\epsilon+2\tilde{\epsilon}+\frac{3}{2})},
\end{aligned}
$$

$$
\begin{aligned}
\boldsymbol{I}^{++}_{(1+2\epsilon-2\tilde{\epsilon})1;10011} =& -\frac{i\pi^{5/2}e^{2\gamma\epsilon}2^{-4\tilde{\epsilon}+6\epsilon+2}\csc(\pi\tilde{\epsilon}-3\pi\epsilon)\Gamma(2\tilde{\epsilon}-4\epsilon)\Gamma(3\epsilon-2\tilde{\epsilon}+\frac{1}{2})}{(e^{2i\pi(\epsilon-\tilde{\epsilon})}-1)\Gamma(-2\epsilon)\Gamma(\tilde{\epsilon}-2\epsilon+1)\Gamma(\tilde{\epsilon}-\epsilon+1)\Gamma(2\epsilon-2\tilde{\epsilon}+1)}{}_4F_3\left(\begin{matrix}2\tilde{\epsilon}-4\epsilon,\tilde{\epsilon}-2\epsilon,\tilde{\epsilon}-2\epsilon+\frac{1}{2},2\epsilon+1\\ 2\tilde{\epsilon}-3\epsilon+\frac{1}{2},\tilde{\epsilon}-2\epsilon+1,\tilde{\epsilon}-\epsilon+1\end{matrix}\middle|1\right)\\
&+\frac{i\pi^{5/2}e^{2\gamma\epsilon}2^{-2\tilde{\epsilon}+4\epsilon+2}\Gamma(-2\epsilon)\csc(\pi\tilde{\epsilon}-3\pi\epsilon)\Gamma(-\tilde{\epsilon}+2\epsilon+\frac{1}{2})}{(e^{2i\pi(\epsilon-\tilde{\epsilon})}-1)\Gamma(1-\epsilon)\Gamma(2\tilde{\epsilon}-4\epsilon)\Gamma(\epsilon-\tilde{\epsilon}+1)\Gamma(2\epsilon-2\tilde{\epsilon}+1)}{}_4F_3\left(\begin{matrix}\tilde{\epsilon}-3\epsilon,\frac{1}{2}-\epsilon,-\epsilon,3\epsilon-\tilde{\epsilon}+1\\ \tilde{\epsilon}-2\epsilon+\frac{1}{2},1-\epsilon,\epsilon-\tilde{\epsilon}+1\end{matrix}\middle|1\right)\\
&-\frac{2\pi^{5/2}e^{2\gamma\epsilon-i\pi(\epsilon-\tilde{\epsilon})}\Gamma(\frac{1}{2}-\epsilon)\cos(2\pi\tilde{\epsilon}-5\pi\epsilon)\,\sec(\pi\tilde{\epsilon}-2\pi\epsilon)\Gamma(-2\tilde{\epsilon}+5\epsilon+\frac{3}{2})}{(\sin(\pi\tilde{\epsilon})-\sin(3\pi\tilde{\epsilon}-6\pi\epsilon))\Gamma(2\tilde{\epsilon}-4\epsilon)\Gamma(\epsilon-\tilde{\epsilon}+\frac{3}{2})\Gamma(2\epsilon-\tilde{\epsilon}+\frac{3}{2})\Gamma(3\epsilon-2\tilde{\epsilon}+\frac{3}{2})}\\
&\times{}_4F_3\left(\begin{matrix}\frac{1}{2}-\epsilon,\epsilon-\tilde{\epsilon}+\frac{1}{2},\epsilon-\tilde{\epsilon}+1,5\epsilon-2\tilde{\epsilon}+\frac{3}{2}\\ \epsilon-\tilde{\epsilon}+\frac{3}{2},-\tilde{\epsilon}+2\epsilon+\frac{3}{2},3\epsilon-2\tilde{\epsilon}+\frac{3}{2}\end{matrix}\middle|1\right). \qquad \text{(A1)}
\end{aligned}
$$

The expansion of these functions for small $(\epsilon,\tilde{\epsilon})$ is rather nontrivial. To deal with the two-parameter problem, as explained in the main text, we set $\tilde{\epsilon}=\eta\epsilon$ and expand the boundary conditions for small ϵ. This allows for a systematic cancellation of spurious poles in the integrand. The resulting values are listed below, with some of them obtained through a high-precision numerical evaluation followed by a reconstruction using the PSLQ algorithm [96,97]:

$$
\begin{aligned}
\boldsymbol{I}^{-+}_{(2\epsilon)1;10011} =& \frac{i\pi^2}{\epsilon}-\pi^2(\pi-2i\log(2))-\frac{1}{2}i\pi^2(\pi-2i\log(2))^2\epsilon\\
&+\frac{1}{6}\pi^2(8i(\log^3(2)-140\zeta(3))+\pi^3-12\pi\log^2(2)-6i\pi^2\log(2))\epsilon^2+\mathcal{O}(\epsilon^3),\\
\boldsymbol{I}^{-+}_{(1+2\epsilon)1;10011} =& \frac{5\pi}{3\epsilon^2}+\frac{5i\pi^2}{3\epsilon}-\frac{19\pi^3}{9}+\mathcal{O}(\epsilon),\\
\boldsymbol{I}^{++}_{(2\epsilon)1;10011} =& \frac{i\pi^2}{\epsilon}+\pi^2(\pi+2i\log(2))+\left(\frac{3i\pi^4}{2}+2i\pi^2\log^2(2)+\pi^3\log(4)\right)\epsilon\\
&+\frac{1}{6}\pi^2(8i(\log^3(2)-56\zeta(3))+11\pi^3+12\pi\log^2(2)+18i\pi^2\log(2))\epsilon^2+\mathcal{O}(\epsilon^3),\\
\boldsymbol{I}^{++}_{(1+2\epsilon)1;10011} =& -\frac{\pi}{\epsilon^2}+\frac{i\pi^2}{\epsilon}+\frac{7\pi^3}{9}+\mathcal{O}(\epsilon),\\
\boldsymbol{I}^{-+}_{(1+2\epsilon-2\eta\epsilon)1;10011} =& -\frac{2\pi(\eta-5)}{(\eta-3)(\eta-2)\epsilon^2}+\frac{2i\pi^2(\eta-1)(\eta-5)}{(\eta-3)(\eta-2)\epsilon}+\frac{\pi^3(4\eta^3-32\eta^2+61\eta-38)}{3(\eta-3)(\eta-2)}+\mathcal{O}(\epsilon),\\
\boldsymbol{I}^{++}_{(1+2\epsilon-2\eta\epsilon)1;10011} =& \frac{2\pi}{(\eta-2)\epsilon^2}+\frac{2i\pi^2(\eta-1)}{(\eta-2)\epsilon}+\frac{\pi^3(4\eta^3-32\eta^2+61\eta-38)}{3(\eta-3)(\eta-2)}+\mathcal{O}(\epsilon). \qquad \text{(A2)}
\end{aligned}
$$

After the poles are removed, we can safely reinstate $\eta=\tilde{\epsilon}/\epsilon$, with final expressions becoming rational functions in both ϵ and $\tilde{\epsilon}$ that can be easily expanded near zero.

APPENDIX B: BASIS OF SPECIAL FUNCTIONS

We list below the set of special functions introduced in the main text depending on MPLs up to weight 3:

$$
\begin{aligned}
&\mathcal{G}_1(x)=1,\\
&\mathcal{G}_2(x)=G(0;1-x)+G(2;1-x),\\
&\mathcal{G}_3(x)=G(1;1-x),\\
&\mathcal{G}_4(x)=G(0,1;1-x),\\
&\mathcal{G}_5(x)=G(0;1-x)G(1;1-x)-G(0,1;1-x)+G(1,2;1-x),\\
&\mathcal{G}_6(x)=\frac{1}{2}G(1;1-x)^2,\\
&\mathcal{G}_7(x)=G(1-i,1;1-x)+G(1+i,1;1-x),\\
&\mathcal{G}_8(x)=G(1;1-x)G(2;1-x)-G(1,2;1-x),\\
&\mathcal{G}_9(x)=G(0,0,1;1-x)+\frac{1}{2}G(0,1,1;1-x),
\end{aligned}
$$

$$
\begin{aligned}
\mathcal{G}_{10}(x) &= -\frac{1}{2}G(2;1-x)G(1;1-x)^2 + G(1,2;1-x)G(1;1-x) + G(0;1-x)G(0,1;1-x) - 2G(0,0,1;1-x) \\
&\quad - 2G(0,1,1;1-x) + G(0,1,2;1-x) - G(1,1,2;1-x), \\
\mathcal{G}_{11}(x) &= -G(0,1,1;1-x) + G(0,1-i,1;1-x) + G(0,1+i,1;1-x), \\
\mathcal{G}_{12}(x) &= \frac{1}{2}G(2;1-x)G(1;1-x)^2 - G(1,2;1-x)G(1;1-x) - \frac{1}{2}G(0,1,1;1-x) + G(0,2,1;1-x) \\
&\quad + G(1,1,2;1-x), \\
\mathcal{G}_{13}(x) &= G(1;1-x)G(0,1;1-x), \\
\mathcal{G}_{14}(x) &= \frac{1}{6}G(1;1-x)^3, \\
\mathcal{G}_{15}(x) &= \frac{1}{2}G(0;1-x)G(1;1-x)^2 - G(2;1-x)G(1;1-x)^2 - (G(0,1;1-x) - 2G(1,2;1-x))G(1;1-x) \\
&\quad - G(0,1,1;1-x) - G(1,1,2;1-x), \\
\mathcal{G}_{16}(x) &= G(1,1-i,1;1-x) + G(1,1+i,1;1-x), \\
\mathcal{G}_{17}(x) &= G(1;1-x)(G(1;1-x)G(2;1-x) - G(1,2;1-x)), \\
\mathcal{G}_{18}(x) &= \frac{1}{2}[G(2;1-x)G(1;1-x)^2 + (-2G(1,2;1-x) + G(1-i,1;1-x) + G(1+i,1;1-x))G(1;1-x) \\
&\quad +2G(0,1,1;1-x) + 2G(1,1,2;1-x) - G(1,1-i,1;1-x) - G(1,1+i,1;1-x)], \\
\mathcal{G}_{19}(x) &= -\frac{1}{2}G(2;1-x)G(1;1-x)^2 + G(1,2;1-x)G(1;1-x) + G(0;1-x)(G(1-i,1;1-x) + G(1+i,1;1-x)) \\
&\quad - G(0,1,1;1-x) - G(0,1-i,1;1-x) - G(0,1+i,1;1-x) - G(1,1,2;1-x) - G(1-i,0,1;1-x) \\
&\quad + G(1-i,1,2;1-x) - G(1+i,0,1;1-x) + G(1+i,1,2;1-x), \\
\mathcal{G}_{20}(x) &= \frac{1}{2}G(2;1-x)G(1;1-x)^2 - G(1,2;1-x)G(1;1-x) + G(0,1,1;1-x) + G(1,1,2;1-x) \\
&\quad + G(1-i,1-i,1;1-x) + G(1-i,1+i,1;1-x) + G(1+i,1-i,1;1-x) + G(1+i,1+i,1;1-x), \\
\mathcal{G}_{21}(x) &= \frac{3}{2}G(2;1-x)G(1;1-x)^2 - 3G(1,2;1-x)G(1;1-x) + 3G(0,1,1;1-x) + 3G(1,1,2;1-x) \\
&\quad + G(1-i,0,1;1-x) + G(1-i,2,1;1-x) + G(1+i,0,1;1-x) + G(1+i,2,1;1-x), \\
\mathcal{G}_{22}(x) &= G(2;1-x)G(0,1;1-x) + G(0,1,1;1-x) - G(0,1,2;1-x) - G(0,2,1;1-x) \\
&\quad + \frac{1}{4}[-G(2;1-x)G(1;1-x)^2 + 2G(1,2;1-x)G(1;1-x) - 2G(1,1,2;1-x)], \\
\mathcal{G}_{23}(x) &= -G(2;1-x)G(1;1-x)^2 + 2G(1,2;1-x)G(1;1-x) - G(2;1-x)G(0,1;1-x) \\
&\quad + G(0;1-x)(G(1;1-x)G(2;1-x) - G(1,2;1-x)) + G(2;1-x)G(1,2;1-x) - G(0,1,1;1-x) \\
&\quad + G(0,1,2;1-x) - 2G(1,1,2;1-x) - 2G(1,2,2;1-x), \\
\mathcal{G}_{24}(x) &= -\frac{1}{2}G(2;1-x)G(1;1-x)^2 + G(1,2;1-x)G(1;1-x) \\
&\quad + G(2;1-x)(G(1-i,1;1-x) + G(1+i,1;1-x)) - G(1,1,2;1-x) - G(1-i,1,2;1-x) \\
&\quad - G(1-i,2,1;1-x) - G(1+i,1,2;1-x) - G(1+i,2,1;1-x), \\
\mathcal{G}_{25}(x) &= \frac{1}{4}[G(2;1-x)G(1;1-x)^2 + 2(G(2;1-x)^2 - G(1,2;1-x))G(1;1-x) \\
&\quad -4G(2;1-x)G(1,2;1-x) + 2G(1,1,2;1-x) + 4G(1,2,2;1-x)], \\
\mathcal{G}_{26}(x) &= \frac{1}{2}G(1;1-x)G(2;1-x)^2 - G(1,2;1-x)G(2;1-x) + G(0,0,1;1-x) + G(1,2,2;1-x).
\end{aligned}
\tag{B1}
$$

[1] P. Amaro-Seoane *et al.* (LISA Collaboration), arXiv:1702.00786.
[2] D. Reitze *et al.*, Bull. Am. Astron. Soc. **51**, 035 (2019).
[3] A. Abac *et al.*, J. Cosmol. Astropart. Phys. 03 (2026) 081.
[4] R. A. Porto, arXiv:1703.06440.
[5] T. Damour, P. Jaranowski, and G. Schäfer, Phys. Rev. D **89**, 064058 (2014).
[6] C. Galley, A. Leibovich, R. A. Porto, and A. Ross, Phys. Rev. D **93**, 124010 (2016).
[7] N. T. Maia, C. R. Galley, A. K. Leibovich, and R. A. Porto, Phys. Rev. D **96**, 084065 (2017).
[8] N. T. Maia, C. R. Galley, A. K. Leibovich, and R. A. Porto, Phys. Rev. D **96**, 084064 (2017).
[9] T. Marchand, L. Bernard, L. Blanchet, and G. Faye, Phys. Rev. D **97**, 044023 (2018).
[10] R. A. Porto and I. Rothstein, Phys. Rev. D **96**, 024062 (2017).
[11] S. Foffa and R. Sturani, Phys. Rev. D **100**, 024047 (2019).
[12] S. Foffa, R. A. Porto, I. Rothstein, and R. Sturani, Phys. Rev. D **100**, 024048 (2019).
[13] G. Cho, R. A. Porto, and Z. Yang, Phys. Rev. D **106**, L101501 (2022).
[14] L. Blanchet, G. Faye, Q. Henry, F. Larrouturou, and D. Trestini, Phys. Rev. D **108**, 064041 (2023).
[15] S. Foffa and R. Sturani, Phys. Rev. D **101**, 064033 (2020).
[16] S. Foffa, P. Mastrolia, R. Sturani, C. Sturm, and W. J. Torres Bobadilla, Phys. Rev. Lett. **122**, 241605 (2019).
[17] J. Blümlein, A. Maier, and P. Marquard, Phys. Lett. B **800**, 135100 (2020).
[18] G. L. Almeida, S. Foffa, and R. Sturani, Phys. Rev. D **104**, 124075 (2021).
[19] D. Bini, T. Damour, A. Geralico, S. Laporta, and P. Mastrolia, Phys. Rev. D **103**, 044038 (2021).
[20] J. Blümlein, A. Maier, P. Marquard, and G. Schäfer, Nucl. Phys. **B965**, 115352 (2021).
[21] D. Bini, T. Damour, and A. Geralico, Phys. Rev. D **102**, 024062 (2020).
[22] D. Bini, T. Damour, and A. Geralico, Phys. Rev. D **102**, 024061 (2020).
[23] D. Bini, T. Damour, and A. Geralico, Phys. Rev. D **102**, 084047 (2020).
[24] M. Khalil, A. Buonanno, J. Steinhoff, and J. Vines, Phys. Rev. D **106**, 024042 (2022).
[25] J. Blümlein, A. Maier, P. Marquard, and G. Schäfer, Phys. Lett. B **816**, 136260 (2021).
[26] R. A. Porto, M. M. Riva, and Z. Yang, J. High Energy Phys. 04 (2025) 050.
[27] G. L. Almeida, A. Müller, S. Foffa, and R. Sturani, Phys. Rev. D **112**, 084077 (2025).
[28] G. Cho, B. Pardo, and R. A. Porto, Phys. Rev. D **104**, 024037 (2021).
[29] L. Amalberti, Z. Yang, and R. A. Porto, Phys. Rev. D **110**, 044046 (2024).
[30] D. Bini, T. Damour, S. De Angelis, A. Geralico, A. Herderschee, R. Roiban, and F. Teng, Phys. Rev. D **109**, 125008 (2024).
[31] T. Damour, Phys. Rev. D **94**, 104015 (2016).
[32] T. Damour, Phys. Rev. D **97**, 044038 (2018).
[33] N. E. J. Bjerrum-Bohr, P. H. Damgaard, G. Festuccia, L. Plante, and P. Vanhove, Phys. Rev. Lett. **121**, 171601 (2018).
[34] C. Cheung, I. Z. Rothstein, and M. P. Solon, Phys. Rev. Lett. **121**, 251101 (2018).
[35] D. A. Kosower, B. Maybee, and D. O'Connell, J. High Energy Phys. 02 (2019) 137.
[36] Z. Bern, C. Cheung, R. Roiban, C.-H. Shen, M. P. Solon, and M. Zeng, Phys. Rev. Lett. **122**, 201603 (2019).
[37] G. Kälin and R. A. Porto, J. High Energy Phys. 01 (2020) 072.
[38] G. Kälin and R. A. Porto, J. High Energy Phys. 02 (2020) 120.
[39] G. Cho, G. Kälin, and R. A. Porto, J. High Energy Phys. 04 (2022) 154; 07 (2022) 002.
[40] T. Damour, Phys. Rev. D **102**, 024060 (2020).
[41] G. Kälin and R. A. Porto, J. High Energy Phys. 11 (2020) 106.
[42] G. Kälin, Z. Liu, and R. A. Porto, Phys. Rev. Lett. **125**, 261103 (2020).
[43] G. Kälin, Z. Liu, and R. A. Porto, Phys. Rev. D **102**, 124025 (2020).
[44] Z. Liu, R. A. Porto, and Z. Yang, J. High Energy Phys. 06 (2021) 012.
[45] G. U. Jakobsen, G. Mogull, J. Plefka, and J. Steinhoff, J. High Energy Phys. 01 (2022) 027.
[46] S. Mougiakakos, M. M. Riva, and F. Vernizzi, Phys. Rev. D **104**, 024041 (2021).
[47] G. Kälin, J. Neef, and R. A. Porto, J. High Energy Phys. 01 (2023) 140.
[48] G. U. Jakobsen, G. Mogull, J. Plefka, and B. Sauer, J. High Energy Phys. 10 (2022) 128.
[49] P. Di Vecchia, C. Heissenberg, R. Russo, and G. Veneziano, J. High Energy Phys. 07 (2021) 169.
[50] C. Dlapa, G. Kälin, Z. Liu, and R. A. Porto, Phys. Lett. B **831**, 137203 (2022).
[51] C. Dlapa, G. Kälin, Z. Liu, and R. A. Porto, Phys. Rev. Lett. **128**, 161104 (2022).
[52] C. Dlapa, G. Kälin, Z. Liu, J. Neef, and R. A. Porto, Phys. Rev. Lett. **130**, 101401 (2023).
[53] Z. Bern, J. Parra-Martinez, R. Roiban, M. S. Ruf, C.-H. Shen, M. P. Solon, and M. Zeng, Phys. Rev. Lett. **126**, 171601 (2021).
[54] Z. Bern, J. Parra-Martinez, R. Roiban, M. S. Ruf, C.-H. Shen, M. P. Solon, and M. Zeng, Phys. Rev. Lett. **128**, 161103 (2022).
[55] D. Bini, T. Damour, and A. Geralico, Phys. Rev. D **107**, 024012 (2023).
[56] P. H. Damgaard, E. R. Hansen, L. Planté, and P. Vanhove, J. High Energy Phys. 09 (2023) 183.
[57] C. Dlapa, G. Kälin, Z. Liu, and R. A. Porto, J. High Energy Phys. 08 (2023) 109.
[58] A. Klemm, C. Nega, B. Sauer, and J. Plefka, Phys. Rev. D **109**, 124046 (2024).
[59] H. Frellesvig, R. Morales, and M. Wilhelm, Phys. Rev. Lett. **132**, 201602 (2024).
[60] Z. Bern, E. Herrmann, R. Roiban, M. S. Ruf, and M. Zeng, J. High Energy Phys. 06 (2025) 115.

[61] Z. Bern, E. Herrmann, R. Roiban, M. S. Ruf, A. V. Smirnov, V. A. Smirnov, and M. Zeng, J. High Energy Phys. 10 (2024) 023.
[62] A. Buonanno, G. U. Jakobsen, and G. Mogull, Phys. Rev. D **110**, 044038 (2024).
[63] C. Dlapa, G. Kälin, Z. Liu, and R. A. Porto, Phys. Rev. Lett. **132**, 221401 (2024).
[64] C. Dlapa, G. Kälin, Z. Liu, and R. A. Porto, Phys. Rev. Lett. **135**, 251401 (2025).
[65] C. Cheung, J. Parra-Martinez, I. Z. Rothstein, N. Shah, and J. Wilson-Gerow, J. High Energy Phys. 10 (2024) 005.
[66] D. Bini and T. Damour, Phys. Rev. D **110**, 064005 (2024).
[67] M. Driesse, G. U. Jakobsen, G. Mogull, J. Plefka, B. Sauer, and J. Usovitsch, Phys. Rev. Lett. **132**, 241402 (2024).
[68] M. Driesse, G. U. Jakobsen, A. Klemm, G. Mogull, C. Nega, J. Plefka, B. Sauer, and J. Usovitsch, Nature (London) **641**, 603 (2025).
[69] C. Heissenberg, Phys. Rev. D **111**, 126012 (2025).
[70] C. Heissenberg and R. Russo, arXiv:2511.13835.
[71] D. Bini and T. Damour, Phys. Rev. D **112**, 044002 (2025).
[72] Z. Bern, E. Herrmann, R. Roiban, M. S. Ruf, A. V. Smirnov, S. Smith, and M. Zeng, arXiv:2512.23654.
[73] L. Blanchet, G. Faye, E. Seraille, and D. Trestini, Classical Quantum Gravity **43**, 105009 (2026).
[74] M. Driesse, G. U. Jakobsen, G. Mogull, C. Nega, J. Plefka, B. Sauer, and J. Usovitsch, arXiv:2601.16256.
[75] W. D. Goldberger and I. Z. Rothstein, Phys. Rev. D **73**, 104029 (2006).
[76] R. A. Porto, Phys. Rev. D **73**, 104031 (2006).
[77] W. Goldberger and I. Rothstein, Phys. Rev. D **73**, 104030 (2006).
[78] R. A. Porto, Phys. Rev. D **77**, 064026 (2008).
[79] R. A. Porto and I. Z. Rothstein, Phys. Rev. D **78**, 044012 (2008).
[80] R. A. Porto and I. Z. Rothstein, Phys. Rev. D **78**, 044013 (2008).
[81] I. Z. Rothstein, Gen. Relativ. Gravit. **46**, 1726 (2014).
[82] R. A. Porto, Phys. Rep. **633**, 1 (2016).
[83] W. D. Goldberger, arXiv:2206.14249.
[84] F. Lange, J. Usovitsch, and Z. Wu, Comput. Phys. Commun. **322**, 109999 (2026).
[85] A. V. Smirnov and M. Zeng, arXiv:2510.07150.
[86] R. N. Lee, J. Phys. Conf. Ser. **523**, 012059 (2014).
[87] R. A. Porto and M. M. Riva, arXiv:2604.09545.
[88] G. Brunello, M. K. Mandal, P. Mastrolia, R. Patil, M. Pegorin, J. Ronca, S. Smith, J. Steinhoff, and W. J. Torres Bobadilla, arXiv:2512.19498.
[89] G. Brunello, M. K. Mandal, P. Mastrolia, R. Patil, M. Pegorin, S. Smith, and J. Steinhoff, arXiv:2604.14134.
[90] G. U. Jakobsen, G. Mogull, J. Plefka, and B. Sauer, Phys. Rev. Lett. **131**, 241402 (2023).
[91] G. U. Jakobsen, G. Mogull, J. Plefka, B. Sauer, and Y. Xu, Phys. Rev. Lett. **131**, 151401 (2023).
[92] L. de la Cruz and D. A. Kosower, arXiv:2602.22111.
[93] J. M. Henn, Phys. Rev. Lett. **110**, 251601 (2013).
[94] R. Jinno, G. Kälin, Z. Liu, and H. Rubira, J. High Energy Phys. 07 (2023) 181.
[95] See Supplemental Material at http://link.aps.org/supplemental/10.1103/wkp4-vy6g for computer-readable ancillary files.
[96] D. Bailey and H. Ferguson, NASA Technical Report RNR-91-032, 1991.
[97] D. H. Bailey and D. J. Broadhurst, Math. Comput. **70**, 1719 (2001).